Solving Fluctuation-Enhanced Poisson-Boltzmann Equations

Zhenli Xu

Department of Mathematics, Institute of Natural Sciences, and MoE Key Lab of Scientific and Engineering Computing, Shanghai Jiao Tong University, 800 Dongchuan Rd., Shanghai 200240, China

A. C. Maggs

Laboratoire de Physico-Chime Théorique, ESPCI, CNRS Gulliver, 10 Rue Vauquelin, 75005,Paris,France

Abstract

Electrostatic correlations and fluctuations in ionic systems can be described within an extended Poisson-Boltzmann theory using a Gaussian variational form. The resulting equations are challenging to solve because they require the solution of a non-linear partial differential equation for the pair correlation function. This has limited existing studies to simple approximations or to one-dimensional geometries. In this paper we show that the numerical solution of the equations is greatly simplified by the use of selective inversion of a finite difference operator which occurs in the theory. This selective inversion preserves the sparse structure of the problem and leads to substantial savings in computer effort. In one and two dimensions further simplifications are made by using a mixture of selective inversion and Fourier techniques.

Keywords: Electrostatic correlation, Variational field theory, Green's function, Poisson-Boltzmann theory, Fast algorithm, Sparse matrix, Selected inversion

1. Introduction

Electrostatic phenomena are important in many fields of engineering, physical and biological sciences. Examples where their study is crucial to the understanding of the large scale properties of materials include colloidal suspensions, electrochemical energy devices, DNA and membrane function, and nano-particle interactions [1, 2, 3]. Classical Poisson-Boltzmann theory [4, 5] is a widespread approach for understanding phenomena in such systems, but it is a mean-field approach which determines the ion concentrations by the average electrostatic potential; it ignores many-body effects and fluctuations. One simple example of the weakness of the standard Poisson-Boltzmann is given by the example of an air-water interface where the equations eliminate self-energy effects and image charges [6, 7]. The density profile predicted by the equations is then a poor approximation close to the surface.

One measure of many-body effect in charged systems is the coupling parameter Ξ, [8], an a-dimensional parameter calculated from surface charge density, σe, counter-ion valency q, dielectric permittivity ϵ and inverse temperature β. In SI units,

$$\Xi = q^3 |\sigma| e^4 \beta^2 / 8\pi\epsilon^2,$$

with e the electronic charge. In the weak-coupling regime, $\Xi \to 0$; the mean-field, Poisson-Boltzmann theory works rather well. In the strong-coupling limit, $\Xi \to \infty$, other theoretical approaches have been developed starting from a single ion picture [9, 1, 10]. This strong-coupling theory successfully captures phenomena such as counterion condensation, and like-charge attraction. The perturbative expansion in either small Ξ or large Ξ can not be applied however for the intermediate regime $\Xi \sim 1$, which is however often found experimentally.

By the use of a Gaussian variation *ansatz*, Netz and Orland [11, 12] derived a system of self-consistent partial differential equations which are believed useful for a larger range of Ξ. Historically, the equations were also derived by Avdeev and Martynov using the Debye closure of the BBGKY hierarchical chain [13]. Based on the self-consistent equations, there has been recent interest of numerical methods and analysis with one-loop expansion or asymptotic approximation; See Buyukdagli *et al.* [14, 15], and references therein; these studies show excellent agreement with Monte Carlo simulations. The variational field-theoretical approach has been discussed by many other authors: [16, 17, 18]. Clearly the equations contain much useful physics and it would be useful to have a tool to study them in more general geometries.

The main result of the present paper is the presentation of numerical methods that enable one to *solve* the self-consistent equations in general geometries. To do this

we firstly discretise the variational equations. When we do so we see that the main technical difficulty that has to be overcome is the inversion of a large system of linear equations. However, closer examination shows that we only require diagonal elements of the inverse matrix, this diagonal inverse is related to a local electrostatic energy of an ion, similar to a spatially varying Born energy [6]. The matrix equations in the self-consistent formulation are *sparse* in structure – that is, they are matrices for which almost all entries are zero. We thus use techniques developed to *selectively invert* [19, 20] the matrices which occur in our problem. This selective inversion requires less memory storage and also less computer operations to perform than the usual algorithms which calculate the full, dense solution of the linear system. This selected inversion is then used as part of an iterative solver to find the self-consistent solution of the full extended Poisson-Boltzmann equations.

The small workstation which we used for our implementation limits us to modest system sizes in arbitrary three-dimensional geometries. However, if we study physical systems which are invariant in one, or two dimensions we can do much better. We give as an example of the interaction between two charged cylinders (2+1 dimensions), or the profile of density near a planar wall (1+2 dimensions). In these cases we can combine the method of selective inversion with Fourier analysis in the invariant directions. Then rather fine discretisations are possible even with modest computational resources. We find that we are able to then generate numerical solutions of the equations for $0 < \Xi < 4.7$, which includes rich physics, but does not reach the regime of like-charge attraction.

To be fully useful in three dimensions, more efficient, multiprocessor, codes will be needed. However, several groups are working on scalable selected inversion [21, 20]. We can expect rather rapid progress on the application to three dimensions. We note that the utility of sparse matrix methods for free energy calculations has already been noted in the calculation of fluctuation based interaction such as van der Waals interactions [22, 23].

2. Self-consistent equations for symmetric electrolytes

We consider a symmetric electrolyte composed of two ion species of valence $\pm q$, in a dielectric medium with fixed charge density $\rho_f(\mathbf{r})$. We assume the ions are point charges, and the ion accessible region Ω has uniform dielectric permittivity; excluded volume effects [24] are ignored in our present paper. We will only allow ions to explore a region with constant dielectric background in order to simplify the treatment of the self energy. We will allow, however, non-fluid regions to have varying dielectric properties in order to describe the electrostatics of membranes or electrodes.

The following two length scales are important for electrolytes. The Bjerrum length, $\ell_B = e^2/(4\pi\varepsilon_0\varepsilon_w k_B T)$,

gives the distance at which two unit point charges have an interaction $k_B T$. Here, ε_0 is the vacuum dielectric permittivity, ε_w is the relative permittivity of water, and the product $k_B T$ is the thermal energy. The Gouy-Chapman length, $\ell_{GC} = 1/(2\pi\ell_B q|\sigma_s|)$, describes the interaction between a charge and a surface charge of density $\sigma_s e$, i.e., at this length the interaction energy is comparable $k_B T$. Here we suppose that $\sigma_s e$ is the average surface charge density of the charge source $\rho_f(\mathbf{r})$. We note that the coupling parameter can be expressed via a ratio of the lengths, $\Xi = q^2 \ell_B/\ell_{GC}$.

We use dimensionless units by using the natural length ℓ_{GC}, and scaling the surface charge density to $\sigma_s \ell_{GC}^2$. In the variational field theory, the grand-canonical partition function is represented by the functional integral $Z = \frac{1}{Z_G} \int \mathcal{D}\phi \exp\{-H[\phi]/\Xi\}$, where Z_G is a normalization factor, $i\phi$ is the fluctuating electrostatic potential and the Hamiltonian functional is [12],

$$H[\phi] = \int \frac{d\mathbf{r}}{2\pi} \left[\frac{(\nabla\phi)^2}{4} + i\phi\rho_f - \frac{\Lambda}{2} e^{\Xi G_0(\mathbf{r},\mathbf{r})/2} \cos\phi \right].$$

Here, the ions contribute only in the accessible region Ω, $\Lambda = 2\lambda/(\pi\sigma_s^2\ell_B)$ is the rescaled fugacity, and λ is a constant related to the chemical potential of symmetric ions. We will also introduce $G_0(\mathbf{r},\mathbf{r}') = 1/|\mathbf{r} - \mathbf{r}'|$, the bare Coulomb potential, in a uniform dielectric background. We have already implicitly regularised the theory, since $G(\mathbf{r},\mathbf{r})$ is divergent in the continuum limit. The term in $\Xi G_0(\mathbf{r},\mathbf{r})/2$ shifts the zero of the chemical potential of the ions.

The variational method uses a general Gaussian Hamiltonian and optimises over the mean and covariance. Explicitly we write,

$$H_0[\phi] = \frac{1}{2} \int\int d\mathbf{r}d\mathbf{r}'[\phi(\mathbf{r})+i\Phi(\mathbf{r})](\Xi G)^{-1}(\mathbf{r},\mathbf{r}')[\phi(\mathbf{r}')+i\Phi(\mathbf{r})'],$$

with Φ the mean potential, and the Green's function G is the covariance. The estimated Gibbs free energy is given by

$$\mathcal{F}_{\text{Gibbs}} = \mathcal{F}_0 + \langle H - H_0 \rangle_0/\Xi,$$

where $\mathcal{F}_0 = -\frac{1}{2}\text{Tr}\log G$ and $\langle\cdot\rangle_0$ is the average with respect to H_0. One finds,

$$\mathcal{F}_{\text{Gibbs}} = -\frac{1}{2}\text{Tr}\log(\Xi G) - \int d\mathbf{r} \left[\frac{(\nabla\Phi)^2}{8\pi\Xi} - \frac{\rho_f\Phi}{2\pi\Xi} \right]$$
$$+ \int\int d\mathbf{r}d\mathbf{r}'\delta(\mathbf{r},\mathbf{r}')\frac{\nabla_\mathbf{r}\nabla_{\mathbf{r}'}G(\mathbf{r},\mathbf{r}')}{8\pi}$$
$$- \frac{\Lambda}{4\pi\Xi}\int d\mathbf{r} e^{-\Xi[G(\mathbf{r},\mathbf{r})-G_0(\mathbf{r},\mathbf{r})]/2}\cosh\Phi. \qquad (1)$$

In this expression we understand the interest in introducing the function G_0 so that the continuum limit is less singular – we expect that the combination $(G(\mathbf{r},\mathbf{r})-G_0(\mathbf{r},\mathbf{r}))$ remains finite.

From the first variation of the free energy functional with respect to the mean potential Φ and the Green's

function $G(\mathbf{r}, \mathbf{r}')$, we obtain the following dimensionless equations (see Appendix Appendix A for the derivation),

$$\nabla^2 \Phi - \Lambda e^{-\Xi c(\mathbf{r})/2} \sinh \Phi = -2\rho_f(\mathbf{r}), \tag{2a}$$

$$\left[\nabla^2 - \Lambda e^{-\Xi c(\mathbf{r})/2} \cosh \Phi \right] G(\mathbf{r}, \mathbf{r}') = -4\pi\delta(\mathbf{r} - \mathbf{r}'), \tag{2b}$$

$$c(\mathbf{r}) = \lim_{\mathbf{r} \to \mathbf{r}'} \left[G(\mathbf{r}, \mathbf{r}') - G_0(\mathbf{r}, \mathbf{r}') \right], \tag{2c}$$

where the space-dependent function $\Xi c(\mathbf{r})/2$ describes the effective self energy of a mobile ion. Since we will solve the variational equations in a discretized form we derive them using the language of matrices and lattice Green functions in Appendix Appendix A.

Eq. (2a) is the modified Poisson-Boltzmann equation where the second term in the left hand side is the density of mobile charge and the right hand side is the density of the fixed charge. These equations are beyond the traditional Poisson-Boltzmann theory. The correlation function $c(\mathbf{r})$ represents the electrostatic energy of a mobile ion interacting with surrounding ions, which is determined by Eqs. (2b) and (2c) self-consistently. Eq. (2b) is a semilinear differential equation in the form of a modified Debye-Hückel equation, where the inverse Debye length, found from $\kappa^2 = \Lambda e^{-\Xi c(\mathbf{r})/2} \cosh \Phi$, depends nonlinearly on c and Φ.

The properties of the system are characterized by two parameters: the coupling parameter $\Xi = q^2 \ell_B / \ell_{GC}$ and the rescaled fugacity $\Lambda = 8\pi\lambda\ell_{GC}^3 \Xi$. We can see that the equations can be decoupled in the small Ξ limit, when they reduce to the classical Poisson-Boltzmann equation. The fugacity is actually a measure of ratio between the Debye screening length and the Gouy-Chapman length, and nonlinear effects come out for $\Lambda \ll 1$ where the Debye-Hückel theory does not work and the generalised equation Eq. (2b) should be adopted.

3. The two-level iterative algorithm

In this section, we discuss the self-consistent iterative scheme, and the algorithm for the modified Poisson-Boltzmann equation.

In the region outside Ω where we suppose the dielectric permittivity is ε_d, the equations for the potential and the Green's function are decoupled,

$$\begin{cases} \eta_\varepsilon \nabla^2 \Phi = -2\rho_f(\mathbf{r}), \\ \eta_\varepsilon \nabla^2 G(\mathbf{r}, \mathbf{r}') = -4\pi\delta(\mathbf{r} - \mathbf{r}'), \end{cases} \tag{3}$$

where $\eta_\varepsilon = \varepsilon_d / \varepsilon_w$ is the relative permittivity. We define the indicator function of the ion accessible region,

$$\chi(\mathbf{r}) = \begin{cases} 1, & \text{if } \mathbf{r} \in \Omega, \\ 0, & \text{otherwise}, \end{cases} \tag{4}$$

and define the relative dielectric function of the space by using the bulk water permittivity ε_w, i.e.,

$$\eta(\mathbf{r}) = \eta_\varepsilon + (1 - \eta_\varepsilon) \chi.$$

Then the governing equation for the whole space can be written as,

$$\begin{cases} \nabla \cdot \eta(\mathbf{r})\nabla\Phi - \chi\Lambda e^{-\Xi c(\mathbf{r})/2} \sinh \Phi = -2\rho_f(\mathbf{r}), \\ \left[\nabla \cdot \eta(\mathbf{r})\nabla - \chi\Lambda e^{-\Xi c(\mathbf{r})/2} \cosh \Phi \right] G = -4\pi\delta(\mathbf{r} - \mathbf{r}'), \\ c(\mathbf{r}) = \lim_{\mathbf{r} \to \mathbf{r}'} \left[G(\mathbf{r}, \mathbf{r}') - G_0(\mathbf{r}, \mathbf{r}')/\eta(\mathbf{r}) \right], \end{cases} \tag{5}$$

where the continuity conditions across the interface $\partial\Omega$ are implied by the operator $\nabla \cdot \eta(\mathbf{r})\nabla$.

We develop a self-consistent iterative scheme for the solution of the partial differential equations (5). The iterative scheme is composed of two alternating steps: For given $c(\mathbf{r})$, solve the modified Poisson-Boltzmann equation (the first equation) for Φ subject to given boundary conditions; and for given $c(\mathbf{r})$ and Φ, solve the modified Debye-Hückel equation (the second equation) for G and then a new $c(\mathbf{r})$. For convenience, we call them the PB and DH steps, respectively. These two steps are iteratively performed until the convergence criteria of the solution is reached. Mathematically, the iterative scheme is expressed by,

$$\begin{cases} \nabla \cdot \eta(\mathbf{r})\nabla\Phi^{(k+1)} - \Lambda e^{-\frac{\Xi c^{(k)}}{2}} \sinh \Phi^{(k+1)} = -2\rho_f(\mathbf{r}), \\ \left[\nabla \cdot \eta(\mathbf{r})\nabla - \Lambda e^{-\frac{\Xi c^{(k)}}{2}} \cosh \Phi^{(k+1)} \right] G^{(k+1)} = -4\pi\delta(\mathbf{r} - \mathbf{r}'), \\ c^{(k+1)}(\mathbf{r}) = \lim_{\mathbf{r} \to \mathbf{r}'} \left[G^{(k+1)}(\mathbf{r}, \mathbf{r}') - G_0(\mathbf{r}, \mathbf{r}')/\eta(\mathbf{r}) \right], \end{cases} \tag{6}$$

for $k = 0, 1, \cdots, K$, where the superscript (k) represents the kth iteration step. The stop criteria is

$$\max |\Phi^{(K)} - \Phi^{(K-1)}| < \delta,$$

where δ is a small pre-set value.

We see, at the kth step, the modified Poisson-Boltzmann equation is still a nonlinear equation, which will be solved by iterative scheme, too, therefore the numerical algorithm for the self-consistent equations is a two-level iterative scheme. The modified Debye-Hückel equation becomes an equation which can be solved by an explicit algorithm, which will be discussed in the next section.

We present the sub-level iterative algorithm, used to solve the modified Poisson-Boltzmann equation. The method in the PB step has been widely studied in literature [25, 26]. We use an iterative algorithm based on a three-point finite-difference discretisation for second-order differentiations of variable coefficients [27], which remains the continuity of electric displacement across the interface. We write the equation in the form,

$$\nabla \cdot \eta(\mathbf{x})\nabla\Phi - f(\mathbf{x}) \sinh \Phi = -2\rho_f(\mathbf{x}), \tag{7}$$

with $f > 0$ being space-dependent function, and $\mathbf{x}$ is a d dimensional variable.

Let h be the mesh size. The d-dimensional mesh is composed of n^d lattice sites where n is the number of grid points in each direction. We define by Ψ the vectorization of the potential values at lattice sites and define by

3

$H_1, \cdots, H_d$ the vectorization of the dielectric permittivity at half integer grids at corresponding dimension and integer grids at other dimensions, with periodic boundary conditions. For example, in two dimensions,

$$\Psi = \{\Phi_{ij}, i, j = 1, \cdots, N\},$$

and

$$H_1 = \{\eta_{i+1/2,j}, i, j = 1, \cdots, n\},$$
$$H_2 = \{\eta_{i,j+1/2}, i, j = 1, \cdots, n\}.$$

We suppose these vectors are column vectors.

Let $\mathbf{D}$ and $\mathbf{D}^T$ be the difference matrices of operators $\nabla \cdot$ and $-\nabla$, where $\mathbf{D} = [\mathbf{D}_1, \cdots, \mathbf{D}_d]$ is of $n^d \times dn^d$ dimensions. Then we can discretize the modified Poisson-Boltzmann equation by,

$$\left[-\mathbf{D}\mathbf{H}\mathbf{D}^T - \mathrm{diag}\{\Gamma^{(l)}\} \right] \Psi^{(l+1)} = R^{(l)}, \qquad (8)$$

where $\mathrm{H} = \mathrm{diag}\{H_1^T, \cdots, H_d^T\}$ and $\mathrm{diag}\{\cdot\}$ is the diagonal matrix with the vectorial argument as the main diagonals, Γ is the vectorial representation of the relaxation function

$$\gamma(\mathbf{x}) = f(\mathbf{x}) \left| \sinh \Phi \right| / \left(|\Phi| + \epsilon \right) \geq 0,$$

with $\epsilon = 10^{-8}$, and R is the vector for the function on the right hand side,

$$r(\mathbf{x}) = f \sinh \Phi - \gamma \Phi - 2\rho_f.$$

In real problems, the fixed charge ρ_f are often point or surface charge, and should be distributed into the lattice sites. In our calculations, the surface charge (for instance on a curves surface) is first discretised into point charges, say of fractional valencies, q_m, $m = 1, \cdots, M$. Each point charge is distributed into the nearest grid sites by a linear weighting function [27],

$$\Delta \rho_{i_1 \cdots i_d} = q_m \prod_{l=1}^{d} \left(1 - \frac{|x_{m,l} - x_{i_l}|}{h} \right), \qquad (9)$$

where $x_{m,l}$ is the lth coordinate of the mth charge, and x_{i_l} is the lth coordinate of one of the nearest lattice sites. Then $\rho_{i_1 \cdots i_d}$ is the superposition of all fractional contributions of point source charges.

The discretisation yields symmetric and negatively definite coefficient matrix, and thus the equations can be efficiently solved by standard direct solvers. We use sparse matrix division in Matlab in our implementation.

4. The generalized Debye-Hückel equation

The greatest difficulty in solving the self-consistent equations arises from the modified DH equation, which can be reformulated during the self-consistent iteration as,

$$[\nabla \cdot \eta(\mathbf{r})\nabla - p(\mathbf{r})] G(\mathbf{r}, \mathbf{r}') = -4\pi\delta(\mathbf{r} - \mathbf{r}'), \qquad (10)$$

where $p(\mathbf{r})$ is given by the previous iteration step. In three dimensions, we can approximate the equation by,

$$\mathbf{A}\mathbf{G} = \mathbf{I}, \qquad (11)$$

where

$$\mathbf{A} = \frac{1}{4\pi h^3} \left[\mathbf{D}\mathbf{H}\mathbf{D}^T + \mathrm{diag}\{P\} \right], \qquad (12)$$

P is the vector of function $p(\mathbf{r})$, $\mathbf{G}$ is a matrix representing lattice Green's function, and $\mathbf{I}$ is unit matrix. We see that the solution for the lattice Green's function is simply equivalent to a matrix inversion, $\mathbf{G} = \mathbf{A}^{-1}$. Let C be the vector of correlation function $c(\mathbf{r})$, $\mathbf{G}_0$ be the lattice Green's function in the free space, and H_0 is the vector of dielectric permittivity defined at integer lattice sites, then we can represent C by,

$$C = \mathrm{diag}(\mathbf{G}) - \mathrm{diag}(\mathbf{G}_0)/H_0. \qquad (13)$$

Here $\mathrm{diag}(\cdot)$ is the vector from diagonals of the argument matrix, to distinguish it from $\mathrm{diag}\{\cdot\}$, and the division between vectors is Hadamard division (entrywise division).

4.1. General remarks on matrix inversion

The solution of Eq. (11) is the bottleneck of numerical calculation with the variational field-theoretical equations. One way of inverting a symmetric and positive definite matrix is by the Cholesky or LDL factorisation, $\mathbf{A} = \mathbf{L}\mathbf{\Lambda}\mathbf{L}^T$, where $\mathbf{L}$ is a lower triangular matrix and $\mathbf{\Lambda}$ is a diagonal matrix; then one computes the inversion $\mathbf{A}^{-1}$ from $\mathbf{L}^{-1}$ and $\mathbf{\Lambda}^{-1}$. Since $\mathbf{A}$ is n^d-by-n^d, the LDL factorization has complexity $O(n^{3d})$ arithmetic operations and $O(n^{2d})$ for storage if dense matrix algorithms are used. Both are prohibitive for multidimensional problems. However, $\mathbf{A}$ is sparse and has small band width. By optimising the ordering for evaluating the Cholesky factors, the saving of the computation can be remarkable [28, 29]. When $d = 2$, the factorisation can be performed with $O(n^3)$ arithmetic operations and $O(n^2)$ storage. When $d = 3$, one requires $O(n^6)$ operations and $O(n^4)$ storage.

Another property that simplifies the problem is that only the diagonal of $\mathbf{G}$ is needed for the modified Poisson-Boltzmann equation. In this case, the complexity for inversion can also be lowered, because $\mathrm{diag}(\mathbf{A}^{-1})$ can be extracted by using the Schur complements recursively produced in the intermediate steps of the LDL factorization. The recent developed SelInv package [19] has provides code to extract the diagonals of a matrix inverse. It permits the calculation of the diagonals of the matrix inverse with the same complexity as the factorisation quoted above. This gain in efficiency is enough for one to be able to selectively invert rather large two-dimensional discretisations of physical problems. The complexity remains rather high for general three dimensional problems; however, in systems with translational invariance we will now show how to combine selective inversion with Fourier analysis.

4.2. One-dimensional geometry

Planar interfaces are often studied to investigate the properties of liquid-liquid interfaces and liquid-solid interfaces of different systems. We present the dimension reduction for one-dimensional geometry in this section, which may be useful in, e.g., theoretical and computational studies of planar electric double layers and nanopores.

We assume η depends only on z coordinate. If the surface charges are uniformly distributed on planes perpendicular to $x - y$ directions, the potential and the self Green's function will be translational invariant. Then we can assume $p(\mathbf{r}) = p(z)$, too. The generalized DH equation can be written into,

$$\nabla \cdot \eta(z) \nabla G(\mathbf{r}, \mathbf{r}') = p(z) G(\mathbf{r}, \mathbf{r}') - 4\pi \delta(\mathbf{r} - \mathbf{r}'). \quad (14)$$

If we do the polar symmetric Fourier transform to the Green's function equation in the $x - y$ plane, we obtain the decoupled one-dimensional equation for each k,

$$\left[\partial_z \eta(z) \partial_z - \eta(z) k^2 - p(z) \right] \hat{G}(k; z, z') = -2\delta(z - z'), \quad (15)$$

where the coefficient of the delta function becomes -2 because the two-dimensional Fourier transform to x and y comes out a $1/2\pi$.

We know well how to solve Eq. (15) by discretizing it in a similar form of (12) such that the one-dimensional lattice Green's function at spatial frequency k is

$$\hat{\mathbf{G}}(k) = 2h \left[\mathbf{D} \mathbf{H} \mathbf{D}^T + \text{diag}\{k^2 H_0 + P\} \right]^{-1}, \quad (16)$$

with $\mathbf{D}$ and $\mathbf{H}$ being the matrices of one dimensional case. On the other hand, we can represent the lattice Green's function in free space as,

$$\hat{\mathbf{G}}_0(k) = 2h \left[\mathbf{D} \mathbf{D}^T + k^2 \mathbf{I} \right]^{-1}. \quad (17)$$

The inverse Fourier transform is

$$G(\mathbf{r}, \mathbf{r}') = \int_0^\infty \hat{G}(k; z, z') J_0(k\rho) k \, dk,$$

where J_0 is the Bessel function, and thus we find the vector of the correlation function (in the case of $\rho = 0$),

$$C = \int_0^\infty \left[\text{diag}\{\hat{\mathbf{G}}(k)\} - \frac{\text{diag}\{\hat{\mathbf{G}}_0(k)\}}{H_0} \right] k \, dk, \quad (18)$$

where the vector division of the second term in the integrand is Hadamard division.

The free-space Green's function has explicit solution. However, it is beneficial to calculate it by Eq. (17) in an approximate way, which gains a singularity cancellation between $\hat{\mathbf{G}}(k)$ and $\hat{\mathbf{G}}_0(k)$, leading to an accurate approximation to C.

Since the integrand has the property of fast decay, the numerical integration (18) can be done by a cutoff at a certain frequency $k = K$. We use a variable transformation $k = e^{\mu v} - 1$, where $\mu > 0$ is a constant parameter, and do the integration on $v \in [0, V]$ with $V = \frac{1}{\mu} \log(K + 1)$ by a Legendre-Gauss quadrature, and find a small number of quadrature points can provide high accuracy.

4.3. Two-dimensional geometry

Suppose the electric potential and the self Green's function is uniform in z direction, which is often considered for cylindrical geometries, e.g., DNA-DNA interaction or charge transport inside a nanotube. Similar to one dimension, we have $\eta(\mathbf{r}) = \eta(x, y)$ and $p(\mathbf{r}) = p(x, y)$, and thus the modified DH equation becomes,

$$\nabla \cdot \eta(x, y) \nabla G(\mathbf{r}, \mathbf{r}') = p(x, y) G(\mathbf{r}, \mathbf{r}') - 4\pi \delta(\mathbf{r} - \mathbf{r}'), \quad (19)$$

which is essentially still a three-dimensional problem with coefficients being invariant in z direction.

We can use the Fourier transform in z direction to reduce the equation into a two dimensional problem. Suppose $\tilde{G}(\omega; x, y; x', y')$ is the transform of G. Then,

$$\left[\nabla_{xy} \cdot \eta \nabla_{xy} - \eta \omega^2 - p \right] \tilde{G}(k; z, z') = -\sqrt{8\pi} \delta(x - x', y - y'), \quad (20)$$

which can be solved by,

$$\tilde{\mathbf{G}}(\omega) = \sqrt{8\pi} h^2 \mathbf{A}(\omega)^{-1}, \quad \text{and,}$$
$$\mathbf{A}(\omega) = \mathbf{D} \mathbf{H} \mathbf{D}^T + \text{diag}\{\omega^2 H_0 + P\},$$

where $\mathbf{D}$ and $\mathbf{H}$ are two-dimensional matrices. Since the inverse Fourier transform,

$$G(\mathbf{r}, \mathbf{r}') = \frac{1}{\sqrt{2\pi}} \int_{-\infty}^\infty e^{-i\omega z} \tilde{G}(\omega; x, y; x', y') d\omega, \quad (21)$$

and the matrix $\mathbf{A}(\omega)$ is symmetric and positive definite, the lattice Green's function can be represented by the matrix,

$$\mathbf{G} = \sqrt{\frac{2}{\pi}} \int_0^\infty \tilde{\mathbf{G}}(\omega) d\omega = 4h^2 \int_0^\infty \mathbf{A}(\omega)^{-1} d\omega, \quad (22)$$

and thus the correlation function is approximated by the integral,

$$C = \sqrt{\frac{2}{\pi}} \int_0^\infty \left[\text{diag}\{\tilde{\mathbf{G}}(\omega)\} - \frac{\text{diag}\{\tilde{\mathbf{G}}_0(\omega)\}}{H_0} \right] d\omega, \quad (23)$$

where $\tilde{\mathbf{G}}_0(\omega) = \sqrt{8\pi} h^2 [\mathbf{D} \mathbf{D}^T + \omega^2 \mathbf{I}]^{-1}$ is the matrix of lattice Green's function in free space.

The same method with the Gauss quadrature as for the one-dimensional case could be adopted to approximate the integral.

5. Numerical results

In this section, we perform numerical study on the convergence and speed of the proposed algorithm for electrolytes in three-dimensional space with the presence of one- or two-dimensional charged interfaces. We set a uniform fugacity parameter $\Lambda = 0.2$, and study the solution with different Ξ. In the calculations, the integral in frequency is discretized with parameters $\mu = 1$, $K = 32$ and the number of quadrature points between $[0, K]$ is 10,

which has been verified highly accurate for most of examples except for the example of free energy calculations where 20 quadrature points are used. The correlation function is subtracted by the bulk value in order to ensure that the bulk property does not change with the coupling parameter. The error criteria of the Poisson-Boltzmann solver and the self-consistent iteration are both 10^{-8}. Periodic boundary conditions are used for both the PB and the DH steps. The calculations are performed with a 2.67 GHz Intel 8-core processor and 48 GB memory.

5.1. One planar surface in electrolytes

We consider one dimensional model in a region $[0, L]$ with $L = 32$. In what follows lengths are measured in the natural scaled units – the Gouy-Chapman length, ℓ_{GC}. A charged planar interface is placed at $z = L/2$ separating the electrolyte into two symmetric half spaces. The surface charge density is

$$\rho_f(z) = \delta(z - L/2).$$

The results of two different coupling parameters $\Xi = 1$ and 4 are calculated. To observe the convergence of the numerical algorithm, the $n = 4096$ solution are taken as the reference solution and the maximum error $\max |\Phi - \Phi_{\mathrm{ref}}|$ is measured. Table 1 displays the errors, the iterative steps of the self-consistent scheme, and the execution timings of the two sets of simulations. The "time1" column represents the execution times with the selected inversion, the "time2" is for the direct inversion of the matrix. The error results show a first-order convergence of the algorithm since the lattice representation of the Delta function is first order of accuracy. The number of iterative steps are significantly increased for a larger Ξ, implying more execution time is needed. For the execution timing, the use of selected inversion is already remarkable even for one-dimensional problems, which has several magnitudes of improvement in comparison to the direct inversion.

The case $n = 1024$ corresponds to a rather fine discretisation $h = \ell_{GC}/32$, which can be expected to resolve the structure of the electrolyte with high precession.

Next we investigate the free energy of the variational equations with the same parameters but for a wider range of the coupling parameter. Appendix Appendix B presents the algorithm for the free energy calculation. In order to evaluate the determinant of the lattice Green's function by combining the sparse Cholesky factorisation with the Fourier analysis, we use the eigenvalues of the negative Laplace operator at invariant dimensions, $\lambda_{ij} = 2\left(1 - \cos\frac{\pi i}{N+1}\right) + 2\left(1 - \cos\frac{\pi j}{N+1}\right)$, where $i, j = 1, 2, \cdots, N$ and N is the number of nodes in x and y directions. Suppose $\mathbf{G} = \mathbf{A}^{-1}$ is the original three dimensional lattice Green's function. To obtain is determinant which is the product of all eigenvalues, we decompose the determinant of $\mathbf{A}$ into N^2 components of one-dimensional block corresponding to each given two-dimensional eigenvalue, $(\hat{\mathbf{A}} + \lambda_{ij})$, where $\hat{\mathbf{A}}$ is the discretised matrix in

z direction. Then the determinant can be evaluated via $\det \mathbf{A} = \Pi_{i,j} \det(\hat{\mathbf{A}} + \lambda_{ij})$.

We use $N = 64$ and three meshes, $n = 128, 256$ and 512, and a variable coupling parameter $\Xi = 1 \sim 4.75$. Table 2 shows the results of free energies and iterative steps. It is observed that the solutions blow up near $\Xi = 4.7$ for all three meshes. The finer mesh only has a slight improvement on the convergence near the blowup point. The nonphysical blowup phenomenon may be understandable because the correlation effect between counterions is energetically favorable for the condensation [30]. This implies that, for high coupling parameter, the variational theory should be further modified; e.g., by including the excluded-volume effect of the counterions.

5.2. Two planar interfaces with a sandwiched layer

The second example is the case of two charged planar interfaces separating the space into three parts. The part between the interfaces is low dielectric region, and the two side parts are electrolytes. The computational interval is $[0, L]$ with $L = 32$, where the region of $[0.4L, 0.6L]$ is inaccessible to ions. The dielectric ratio is set to be $\eta(z) = 0.1$ in the region $[0.42L, 0.58L]$ and 1 otherwise, and we see there is a $0.02L$ thickness of buffer zone between the ionic fluid and the dielectric object. This dielectric medium is a model of membrane. We suppose asymmetric unit surface charges are placed at the two ends of the ion inaccessible region, and thus the fixed charge density is

$$\rho_f(z) = \delta(z - 0.4L) - \delta(z - 0.6L).$$

As in the previous example, we first calculate the errors and execution timings with the mesh refinement for two coupling parameters $\Xi = 1$ and 4, shown in Table 3. The first order of accuracy remains, and the convergence of self-consistent iteration is rapid for small Ξ, but becomes worse with the increase of the coupling parameter. Mesh refinement slightly improves the convergence rate.

Table 3: Errors, iterative steps, and execution times (in Seconds) for $\Xi = 1$ and 4 and $n = 128 \sim 1024$. The case of two planar interfaces.

	$\Xi = 1$			$\Xi = 4$		
n	Error	steps	time1	Error	steps	time1
128	0.285	8	0.184	0.344	83	0.861
256	0.139	8	0.265	0.145	45	0.712
512	0.082	8	0.435	0.024	40	1.031
1024	0.028	7	0.753	0.012	36	1.725

We then fix the number of grid points, $N = 1024$, and calculate the results of $\Xi = 1, 2$ and 4. In Fig. 1, we plot the potential distributions, their deviations from the Poisson-Boltzmann solution, the counterion charge densities, and the correlation functions for these three Ξ. Only the left half solutions are plotted due to the symmetry or antisymmetry along $z = L/2$. From (a-b), it is observed that with the increase of coupling parameter, the

Table 1: Errors, iterative steps, and execution times (in Seconds) for $\Xi = 1$ and 4 and $n = 128 \sim 1024$. The case of one planar interface.

	$\Xi = 1$				$\Xi = 4$			
n	Error	steps	time1	time2	Error	steps	time1	time2
128	0.115	7	0.087	1.77	0.123	29	0.268	6.15
256	0.058	7	0.119	6.90	0.068	28	0.366	25.28
512	0.027	7	0.182	29.07	0.033	28	0.550	104.94
1024	0.012	7	0.314	121.96	0.014	27	0.921	425.36

Table 2: Free energies and iterative steps for $\Xi = 1 \sim 4.75$ and $n = 128, 256$ and 512. The case of one planar interface.

	$n = 128$		$n = 256$		$n = 512$	
Ξ	Energy	steps	Energy	steps	Energy	steps
1	0.677	8	0.703	8	0.715	8
2	0.866	12	0.891	12	0.899	12
3	0.944	17	0.968	17	0.976	17
4	1.005	30	1.030	30	1.037	29
4.5	1.049	59	1.074	57	1.080	52
4.6	1.065	89	1.090	86	1.093	70
4.65	1.079	173	1.104	150	1.103	92
4.70	blowup	–	blowup	–	1.120	206
4.75	blowup	–	blowup	–	blowup	–
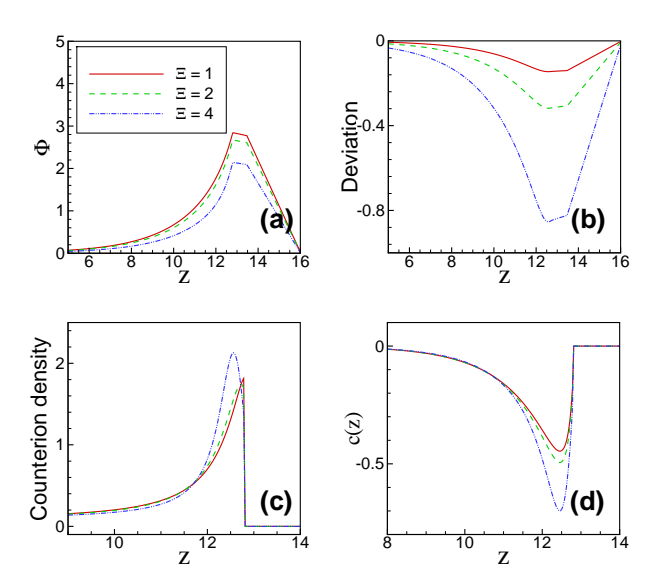
potential magnitude becomes small. It is reasonable in the sense the correlation function $c(\mathbf{r})$ is negative (Fig. 1(d)) and favorable for high counterion concentration. At $\Xi = 2$, we see the deviation of the self-consistent equations from the Poisson-Boltzmann equation is already large, which is over 10% difference at the maximum potential. Another phenomenon we can observe from (c) is that, with the increase of Ξ, the image charge effect is strengthened, which behaviors a repulsive interaction to the counterions.

5.3. Circular geometry

We consider an example of 2D geometry of L^2 with $L = 32$ in units of the Gouy-Chapman length. The electrolyte fills the space outside a circle of radius R. Unit line charge density is placed on this circle, but it has distinct signs in each half surface, i.e.,

$$\rho_f(x, y) = \text{sign}(y)\delta(\sqrt{x^2 + y^2} - R).$$

This setting models a Janus particle. The dielectric ratio η equals 0.1 inside a circle of radius $R - 0.1$, and 1 outside. This 0.1 gap characterizes the size of mobile ions, and eliminates the singularity of computing the correlation function in DH steps.

To see the convergence and execution timings of the algorithms for two dimesions, we take the coupling parameter $\Xi = 4$, and three mesh sizes, 128^2, 256^2 and 512^2. The surface charge is approximated by 128 cations and 128 anions, which are then distributed onto lattice sites. Fig. 2 plots the contours of the potential distributions of three cases, and their potential values at the $x = 0$ line, which show the convergence of the algorithm. Table 4 lists the potential difference between the current step and the previous step at each iteration, and the execution times of the


Figure 1: Results of $\Xi = 1, 2$, and 4 for the case of two planar interfaces. (a) Potential distributions; (b) Potential deviations from the Poisson-Boltzmann solutions; (c) Counterion charge density; (d) Correlation functions.

PB step and the DH step. Only the data of the first 9 iterative steps are given, and overall they are convergent both after ~ 30 steps. It is found that the PB sub-step is very fast after a few iterative steps and most of execution time is spent on the DH steps. For 256^2 and 512^2 meshes, each iterative step for the single processor running can be accomplished in ~ 1 minute and ~ 11 minutes, respectively, even although dozens of selected inversion operations must be performed in order to perform the Fourier integral.
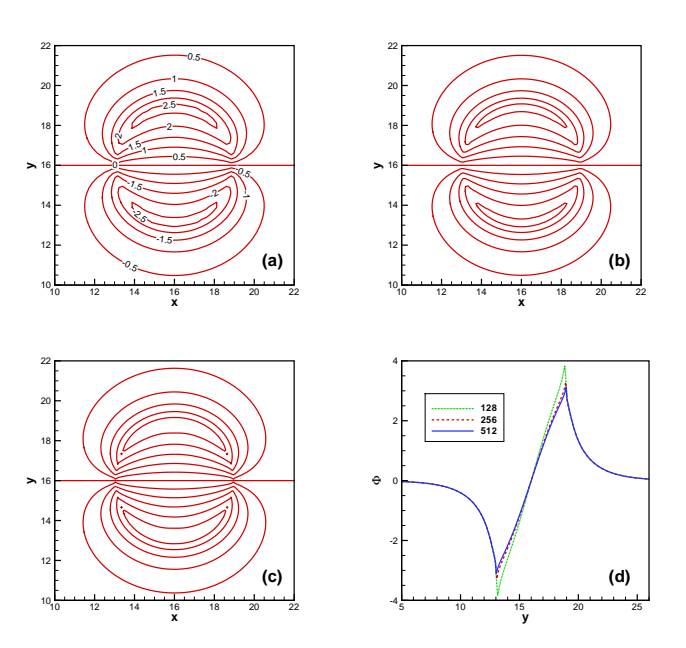
Figure 2: Potential contours of the two dimensional case for (a) 128^2 mesh, (b) 256^2 mesh, and (c) 512^2 mesh; and (d) the potentials at the $x = 0$ line for the three meshes.

We note that we have been unable to use our algorithm to study systems roughly with $\Xi > 5$. We have already shown that convergence is *slower* when Ξ increases, however at some point we find that the iterative process does not converge. This seems to be associated with a condensation of charges to the surface. It is possible that including finite size effects for the ions could prevent this phenomenon, but we leave further study of this point to a later study.

6. Conclusion

We have developed an algorithm for solving fluctuation enhanced Poisson-Boltzmann equations derived using a variational field-theoretic approach. By studying numerical examples, we show the algorithm has attractive performance for both accuracy and efficiency.

For the moment considerations of speed limit detailed studies to one- and two-dimensional geometries. Extension of the algorithm to large three-dimensional geometries is straightforward, but limits to a small mesh (our single-processor machine allows the computation with the 64^3 mesh in a few hours). Exploring the finer mesh solution

requires a parallel implementation of the selected inversion algorithm.

In the framework of self-consistent equations, we aim to include the Born energy contribution to the self energy for charged systems in smoothly varying dielectric media [6] in order to study more complex, heterogeneous materials.

Appendix A. Variational derivation in matrix form

In this appendix we give a derivation of the variational equations starting from a discretised version of the free energy. This derivation is useful because it removes many of the ambiguities and divergences present in the continuum formulation.

Suppose Φ and ρ_f are vectors, $\mathbf{G}$ and $\mathbf{G}_0$ are matrices, and $-\mathbf{D}^T$ is the discrete correspondence of gradient operator. The the matrix operator $\mathbf{D}$ is discretised version of the divergence. Functions of vectors, such as $\cosh\Phi$, correspond to a vector made of the individual elements, in a manner familiar in Matlab. Then in discrete form, the field-theoretic Gibbs free energy can be written as,

$$\mathcal{F}_{\text{Gibbs}} = -\frac{1}{2}\text{Tr}\log(\Xi\mathbf{G}) - \frac{(\mathbf{D}^T\Phi)^T\mathbf{H}\mathbf{D}^T\Phi}{8\pi\Xi}$$
$$+ \text{Tr diag}\left\{\frac{\rho_f \circ \Phi}{2\pi\Xi}\right\} - \text{Tr}\frac{\mathbf{D}\mathbf{H}\mathbf{D}^T\mathbf{G}}{8\pi}$$
$$-\frac{\Lambda}{4\pi\Xi}\text{Tr diag}\left\{e^{-\Xi\Delta G_{rr}/2} \circ \cosh\Phi\right\}, \quad (A.1)$$

where "$\circ$" is the Hadamard product, and $\Delta G_{rr} = \text{diag}(\mathbf{G} - \mathbf{G}_0)$ represent the difference vectors of diagonal elements of $\mathbf{G}$ and $\mathbf{G}_0$. We use matrix derivatives with respect to vector or matrix (e.g., refer to [31]) for the variation with respect to Φ and G.

The variation with respect to Φ gives,

$$\frac{\delta\mathcal{F}_{\text{Gibbs}}}{\delta\Phi} = -\mathbf{D}\frac{\partial\mathcal{F}_{\text{Gibbs}}}{\partial\mathbf{D}^T\Phi} + \frac{\partial\mathcal{F}_{\text{Gibbs}}}{\partial\Phi}$$
$$= -\frac{\mathbf{D}\mathbf{H}\mathbf{D}^T\Phi}{4\pi\Xi} + \text{diag}\left\{\frac{\rho_f}{2\pi\Xi} - \frac{\Lambda}{4\pi\Xi}e^{-\Xi\Delta G_{rr}/2} \circ \sinh\Phi\right\}.$$
$$(A.2)$$

Using $4\pi\Xi\delta\mathcal{F}_{\text{Gibbs}}/\delta\Phi = 0$ yields the modified Poisson-Boltzmann equation,

$$-\mathbf{D}\mathbf{H}\mathbf{D}^T\Phi + \text{diag}\left\{2\rho_f - \Lambda e^{-\Xi\Delta G_{rr}/2} \circ \sinh\Phi\right\} = \mathbf{0}.$$
$$(A.3)$$

Similarly, the variation of the free energy to matrix $\mathbf{G}$ is,

$$\frac{\delta\mathcal{F}_{\text{Gibbs}}}{\delta\mathbf{G}} = -\mathbf{D}\frac{\partial\mathcal{F}_{\text{Gibbs}}}{\partial\mathbf{D}^T\mathbf{G}} + \frac{\partial\mathcal{F}_{\text{Gibbs}}}{\partial\mathbf{G}}$$
$$= \mathbf{D}\frac{\mathbf{H}\mathbf{D}^T\mathbf{I}}{8\pi} - \frac{1}{2\mathbf{G}} + \frac{\Lambda}{8\pi}\text{diag}\left\{e^{-\Xi\Delta G_{rr}/2} \circ \cosh\Phi\right\}.$$
$$(A.4)$$

By $\delta\mathcal{F}_{\text{Gibbs}}/\delta\mathbf{G} = \mathbf{0}$ and right multiplying by $8\pi\mathbf{G}$, we find the generalized Debye-Hückel equation,

$$\mathbf{D}\mathbf{H}\mathbf{D}^T\mathbf{G} + \text{diag}\left\{\Lambda e^{-\Xi\Delta G_{rr}/2} \circ \cosh\Phi\right\}\mathbf{G} = 4\pi\mathbf{I}. \quad (A.5)$$

Table 4: Potential differences and execution times (in Seconds) of the PB and DH steps in the first 9 iterative steps. 128^2, 256^2 and 512^2 meshes.

	128^2 mesh			256^2 mesh				512^2 mesh		
Step	Diff	PB step	DH step	Diff	PB step	DH step	Step	Diff	PB step	DH step
0	3.88336	8.29	3.92	3.32273	45.09	56.48	0	3.10677	239.88	666.14
1	0.15133	1.22	4.22	0.11065	6.25	56.54	1	0.11336	34.88	669.50
2	0.03013	1.19	4.08	0.03376	5.85	56.54	2	0.03271	32.97	669.89
3	0.01704	1.06	4.18	0.01860	5.31	56.39	3	0.01787	31.42	672.02
4	0.00888	1.08	3.92	0.00966	5.37	56.43	4	0.00916	30.77	669.03
5	0.00454	1.02	4.26	0.00498	4.93	58.24	5	0.00466	29.16	667.80
6	0.00235	1.00	4.29	0.00260	5.03	58.34	6	0.00240	28.16	672.96
7	0.00123	0.90	3.92	0.00138	4.53	58.24	7	0.00126	27.41	669.31
8	0.00065	0.89	3.92	0.00074	4.53	56.99	8	0.00067	24.82	668.74

Appendix B. Evaluation of the self-consistent free energy, divergences

The continuum limit of the energy eq. (1) in three dimensions is divergent in $1/h^3$ as the cut-off in the problem, h, is taken to zero. In this appendix we show that this problem is easily solved by always calculating energies compared to an empty system with $\rho_f = 0$ and $\Lambda = 0$. There is also another small problem with the use of eq. (1) in a working code – it requires access to values of G which are near to, but not on the diagonal in order to calculate the derivatives. Selected inversion does not easily give this information so we eliminate the derivative using the variational equations eq. (5):

$$\mathcal{F} = -\frac{1}{2}\mathrm{Tr}\log(\Xi G) - \int d\mathbf{r}\left[\frac{\eta(\nabla\Phi)^2}{8\pi\Xi} - \frac{\rho_f \Phi}{2\pi\Xi}\right]$$
$$- \int d\mathbf{r}\frac{\Lambda\chi}{8\pi\Xi}e^{-\Xi c(\mathbf{r})/2}\cosh\Phi \; G(\mathbf{r},\mathbf{r})$$
$$- \int d\mathbf{r}\frac{\Lambda\chi}{4\pi\Xi}e^{-\Xi c(\mathbf{r})/2}\cosh\Phi$$

where we have dropped a constant coming from the integral of a δ-function. We now shift the zero of free energy taking as a reference,

$$\mathcal{F}_{\mathrm{ref}} = \mathcal{F}(\rho_f = 0, \Lambda = 0), \qquad (\text{B}.1)$$

for the system

$$-\nabla \cdot \eta\nabla G_{\mathrm{ref}} = 4\pi\delta(\mathbf{r} - \mathbf{r}') \qquad (\text{B}.2)$$

If $\eta = 1$ everywhere then $G_{\mathrm{ref}} = G_0$; in a more general background the functions are different.

Firstly we study the behavior of $\mathcal{F} - \mathcal{F}_{\mathrm{ref}}$. Let us consider only the potentially divergent terms:

$$-\frac{1}{2}\mathrm{Tr}\,\log(G/G_{\mathrm{ref}}) - \frac{\Lambda\chi}{8\pi\Xi}e^{-\Xi c(\mathbf{r})/2}\cosh\Phi\; G(\mathbf{r},\mathbf{r}).$$

The last term containing $G(\mathbf{r},\mathbf{r})$ has a naive divergence in $1/h^3$. We now show that this divergence is cancelled by a residual divergence in the logarithmic contribution:

$$-\frac{1}{2}\log(G/G_{\mathrm{ref}}) = \frac{1}{2}\log\left(\frac{-\nabla^2 + \Lambda\chi\cosh\Phi e^{-\Xi c(\mathbf{r})/2}}{-\nabla^2}\right)$$
$$= \frac{1}{2}\log\left(1 + \frac{G_{\mathrm{ref}}}{4\pi\Xi}\Lambda\chi\cosh\Phi e^{-\Xi c(\mathbf{r})/2}\right).$$

Take the trace of this expression. When the eigenvalues of the expression involving G_{ref} are small we can expand the log in a Taylor series to find a contribution:

$$\frac{G_{\mathrm{ref}}}{8\pi\Xi}\Lambda\chi\cosh\Phi\; e^{-\Xi c(\mathbf{r})/2} \qquad (\text{B}.3)$$

We find that the dangerous parts combine to give:

$$\frac{\Lambda\chi}{8\pi\Xi}e^{-\Xi c(\mathbf{r})/2}\cosh\Phi\left[G(\mathbf{r},\mathbf{r}) - G_{\mathrm{ref}}(\mathbf{r},\mathbf{r})\right]. \qquad (\text{B}.4)$$

The combination $G - G_{\mathrm{ref}}$ should remain finite as the mesh spacing goes to zero. Thus $\mathcal{F} - \mathcal{F}_{\mathrm{ref}}$ does too.

Using the variational identity eq. (5) we now find:

$$\mathcal{F} - \mathcal{F}_{\mathrm{ref}} = -\frac{1}{2}\mathrm{Tr}\log(G/G_{\mathrm{ref}}) + \frac{1}{4\pi\Xi}\int d\mathbf{r}\rho_f\Phi +$$
$$\int d\mathbf{r}\frac{\Lambda\chi e^{-\Xi c(\mathbf{r})/2}}{8\pi\Xi}\left[\Phi\sinh\Phi - \cosh\Phi\;\Xi G(\mathbf{r},\mathbf{r}) - 2\cosh\Phi\right].$$

This is our required result: A free energy which remains finite as the cut-off is reduced, and which does not require access to non-diagonal elements of G. Since $\mathrm{Tr}\log = \log\det$, the determinants are calculated rather easily through Cholesky factorisation of the corresponding sparse operator [22].

References

[1] H. Boroudjerdi, Y.-W. Kim, A. Naji, R. R. Netz, X. Schlagberger, A. Serr, Statics and dynamics of strongly charged soft matter, Phys. Rep. 416 (2005) 129–199.

[2] R. H. French, V. A. Parsegian, R. Podgornik, R. F. Rajter, A. Jagota, J. Luo, D. Asthagiri, M. K. Chaudhury, Y.-M. Chiang, S. Granick, S. Kalinin, M. Kardar, R. Kjellander, D. C. Langreth, J. Lewis, S. Lustig, D. Wesolowski, J. S. Wettlaufer, W.-Y. Ching, M. Finnis, F. Houlihan, O. A. von Lilienfeld, C. J. van Oss, T. Zemb, Long range interactions in nanoscale science, Rev. Mod. Phys. 82 (2) (2010) 1887–1944.

[3] A. Naji, M. Kanduč, J. Forsman, R. Podgornik, Perspective: Coulomb fluids – weak coupling, strong coupling, in between and beyond, arXiv: 1307.5130 .

[4] G. Gouy, Constitution of the electric charge at the surface of an electrolyte, J. Phys. 9 (1910) 457–468.

[5] D. L. Chapman, A contribution to the theory of electrocapillarity, Phil. Mag. 25 (1913) 475–481.

[6] Z. G. Wang, Fluctuation in electrolyte solutions: The self energy, Phys. Rev. E 81 (2010) 021501.

[7] M. Kanduč, R. Podgornik, Electrostatic image effects for counterions between charged planar walls, Eur. Phys. J. E 23 (3) (2007) 265–274.

[8] R. R. Netz, Electrostatics of counter-ions at and between planar charged walls: From Poisson-Boltzmann to the strong-coupling theory, The European Physical Journal E: Soft Matter and Biological Physics 5 (1) (2001) 557–574.
URL http://dx.doi.org/10.1007/s101890170039

[9] M. S. Loth, B. I. Shklovskii, Non-mean-field screening by multivalent counterions, Journal of Physics: Condensed Matter 21 (42) (2009) 424104.
URL http://stacks.iop.org/0953-8984/21/i=42/a=424104

[10] L. Šamaj, E. Trizac, Wigner-crystal formulation of strong-coupling theory for counterions near planar charged interfaces, Phys. Rev. E 84 (2011) 041401.
URL http://link.aps.org/doi/10.1103/PhysRevE.84.041401

[11] R. R. Netz, H. Orland, Beyond Poisson-Boltzmann: Fluctuation effects and correlation functions, Eur. Phys. J. E 1 (2000) 203–214.

[12] R. Netz, H. Orland, Variational charge renormalization in charged systems, Eur. Phys. J. E 11 (2003) 301–311.

[13] S. M. Avdeev, G. A. Martynov, Influence of image forces on the electrostatic component of the disjoining pressure, Colloid J. USSR 48 (1986) 535–542.

[14] S. Buyukdagli, M. Manghi, J. Palmeri, Variational approach for electrolyte solutions: From dielectric interfaces to charged nanopores, Phys. Rev. E 81 (2010) 041601.

[15] S. Buyukdagli, C. V. Achim, T. Ala-Nissila, Electrostatic correlations in inhomogeneous charged fluids beyond loop expansion, J. Chem. Phys. 137 (2012) 104902.

[16] A. E. Yaroshchuk, Dielectric exclusion of ions from membranes, Adv.Colloid Interface Sci. 85 (2000) 193–230.

[17] M. M. Hatlo, L. Lue, The role of image charges in the interactions between colloidal particles, Soft Matter 4 (2008) 1582–1596.

[18] A. W. C. Lau, D. B. Lukatsky, P. Pincus, S. A. Safran, Charge fluctuations and counterion condensation, Phys. Rev. E 65 (2002) 051502.

[19] L. Lin, C. Yang, J. C. Meza, J. Lu, L. Ying, W. E, Selinv—An algorithm for selected inversion of a sparse symmetric matrix, ACM Trans. Math. Softw. 37 (2011) 40:1–40:19.

[20] L. Lin, C. Yang, J. Lu, L. Ying, W. E, A fast parallel algorithm for selected inversion of structured sparse matrices with application to 2d electronic structure calculations, SIAM Journal on Scientific Computing 33 (3) (2011) 1329–1351.

[21] P. R. Amestoy, A. Guermouche, J.-Y. L'Excellent, S. Pralet, Hybrid scheduling for the parallel solution of linear systems, Parallel Computing 32 (2) (2006) 136–156.

[22] S. Pasquali, A. C. Maggs, Fluctuation-induced interactions between dielectrics in general geometries, The Journal of Chemical Physics 129 (1) (2008) 014703.

[23] S. Pasquali, A. C. Maggs, Numerical studies of lifshitz interactions between dielectrics, Phys. Rev. A 79 (2009) 020102.

[24] I. Borukhov, D. Andelman, H. Orland, Steric effects in electrolytes: A modified Poisson-Boltzmann equation, Phys. Rev. Lett. 79 (1997) 435–438.

[25] B. Z. Lu, Y. C. Zhou, M. J. Holst, J. A. McCammon, Recent progress in numerical methods for the Poisson-Boltzmann equation in biophysical applications, Commun. Comput. Phys. 3 (2008) 973–1009.

[26] C. Li, L. Li, M. Petukh, E. Alexov, Progress in developing Poisson-Boltzmann equation solvers, Mol. Based Math. Biol. 1 (2013) 42–62.

[27] W. Im, D. Beglov, B. Roux, Continuum solvation model: Computation of electrostatic forces from numerical solutions to the Poisson-Boltzmann equation, Comput. Phys. Commun. 111 (1998) 59–75.

[28] A. George, Nested dissection of a regular finite element mesh, SIAM J. Numer. Anal. 10 (1973) 345–363.

[29] I. Duff, A. Erisman, J. Reid, On George's nested dissection method, SIAM J. Numer. Anal. 13 (1976) 686–695.

[30] Y. Levin, Electrostatic corrections: from plasma to biology, Rep. Prog. Phys. 65 (2002) 1577–1632.

[31] K. B. Petersen, M. S. Pedersen, The matrix cookbook, Version: November 14, 2008.